
A COMPARATIVE STUDY OF HUMAN INVERSE KINEMATICS TECHNIQUES FOR LOWER LIMBS

Zineb BENHMIDOUCH, Saad MOUFID, Aissam AIT OMAR
z.benhmouch@gmail.com

February 23, 2023

ABSTRACT

Inverse Kinematics (IK) has been an active research topic and many methods have been introduced to provide a fast and accurate solution. However, high computational cost and the generation of unrealistic positions constitute the weak points in most existing IK methods. In this paper, a comparative study was established to analyze the performance of popular IK techniques applied to the human leg. The objective is to determine the most efficient method in terms of computation time and to reach the desired position with a realistic human posture while respecting the range of motion and joint comfort zones of every joint.

Keywords Human inverse kinematics · Numerical method · Optimization · Neural network · Genetic algorithm

1 Introduction

One of the most crucial and challenging steps in the development of robots intended to restore the mobility of the human body after a loss of functional movement due to neurological injuries is the IK of physiological limbs, which consists of computing joint angles configuration based on the predefined input workspace coordinates. Generally speaking, the complexity of the IK problem depends on the geometry of the manipulator and the nonlinearity of its model, which gives the corresponding relation between the task and the joint spaces. Furthermore, IK solution is essential for the real-time control. Thus, it must be precise in order to enable the robot to perform the task successfully. IK techniques can be classified into three categories, namely, analytical method, numerical method, and intelligent method.

The analytical method solves IK by solving a set of closed-form equations that can give the generalized coordinate value that drives the end effector of the manipulator to the predefined target position [1]. Furthermore, this method takes into consideration the geometric insight into the problem and the particular structure of the robot. For an arbitrary robot kinematics, the analytic solutions for IK may not exist, or may be multiple. Whereas numerical techniques are iterative methods which converge to only one solution depending on an initial point. There are several algorithms used to solve IK problems, namely, Moore-Penrose pseudo-inverse method [2], cyclic coordinate descent method [3], Levenberg Marquardt damped least squares method [4], optimization method and multi-objective optimization using genetic algorithm [5] and so forth. Moreover, the neural network approach [6] for solving the inverse kinematics is based on the idea of investigating the whole configuration workspace of the robot and selecting the optimal solution.

Indeed, the main advantage of analytical method solution is its accuracy and its efficiency as it delivers results in real-time. In addition, the analytical algorithm computes the valid potential configurations. Nevertheless, the number of solutions is very large when the manipulator has more than 6 degrees of freedom. Moreover, when a solution is impossible, the algorithm would not return an approximate solution that satisfies all the constraints. However, the pseudo-inverse and damped least squares perform very poorly and are slow. Although the cyclic coordinate descent method is simple to implement and computationally fast, but it is difficult to produce smooth motions and consider non-geometric constraints as the minimum energy criteria. While optimization based methods are discrete solve the IK problem by point to point unlike neural network approach.

A set of IK algorithms suitable for the lower limbs were examined in this paper in order to investigate the optimal method regarding efficiency, accurately, computational cost, energy consumption and production of realistic posture. Thus, analytical, numerical and intelligent methods have been used to solve the generalized IK problem taking into

Table 1: Modified D-H parameters for the right lower limb

Joint	α_{i-1}	a_{i-1}	d_i	θ_i
1	0	0	b	θ_1
2	0	L_1	0	$-\theta_2$
3	0	L_2	0	θ_3
4	0	L_3	0	0

consideration position, orientation, and angular constraints.

The rest of this paper is organized as follows. Section 2 describes the mechanical structure, elaborates the forward kinematics and investigates the workspace analysis and trajectory planning of the human lower limb respectively. While Section 3 focuses on application of the different inverse kinematics methods for human leg. Finally, in sections 4 and 5, the simulation results are discussed.

2 ARTICULATED HUMAN LEG MODEL

This section provides a functional description of the lower limbs based on the work of Calais Germain [7]. Firstly, in biomechanics, movements are usually described in a reference which has three planes: sagittal plane (median plane), frontal plane, and transverse plane and three axes named left-right axis (frontal axis), anteroposterior axis (sagittal axis), and craniocaudal axis (superior and inferior axis). In anatomy, the lower limb is decomposed into four segments, the pelvis, the thigh, the leg and the foot, linked together by three joint groups, the hip (or coxofemoral joint), the knee and the ankle. The hip joint rotates around the three perpendicular axes which have been mentioned above. Indeed this articulation has the mechanical characteristic of a spherical joint, i.e. it has three degrees of freedom (DOF). The knee joint permits movement in 1-DOF, flexion-extension in the sagittal plane around left-right axis. While, the ankle joint moves in all three planes, resulting in 3-DOF. So each side of the lower limbs has 7-DOF. However, in this study, we will only consider the movements in the sagittal plane, which means that we will only consider the movements of flexion and extension of each joint. This involves 3-DOF for each side of the lower limbs.

The kinematics of the physiological lower limbs is used to find a relation between the Cartesian coordinates of the big toe E and the generalized coordinate $q = [\theta_1 \ \theta_2 \ \theta_3]^T$. Using the modified Denavit-Hartenberg (D-H) convention, the reference frame at each joint of the lower limbs is described in Figures 1 and 2. Thus, the link parameters of the right kinematic chain is given in Table 1.

Consequently, the relation between the coordinate system of the big toe E and the joint angular displacement is given by the following matrix.

$$T_4^0 = \begin{bmatrix} C_{1-23} & -S_{1-23} & 0 & L_3.C_{1-23} + L_2.C_{1-2} + L_1.C_1 \\ S_{1-23} & C_{1-23} & 0 & L_3.S_{1-23} + L_2.S_{1-2} + L_1.S_1 \\ 0 & 0 & 1 & b \\ 0 & 0 & 0 & 1 \end{bmatrix} \quad (1)$$

Where,

$$C_{1-23} := \cos(\theta_1 - \theta_2 + \theta_3);$$

$$S_{1-23} := \sin(\theta_1 - \theta_2 + \theta_3);$$

$$C_{1-2} := \cos(\theta_1 - \theta_2);$$

$$S_{1-2} := \sin(\theta_1 - \theta_2);$$

$$C_1 := \cos(\theta_1);$$

$$S_1 := \sin(\theta_1);$$

The Monte Carlo method [8] is used to get the feasible workspace of the lower limbs to evaluate its working ability. The principle of the method is as follows: The Monte Carlo method generates pseudo-random number in the interval $[0, 1]$ which respects a uniform distribution. Thereafter, each random sampling generates a set of variable values of the generalized coordinate q by using the following equation:

$$q = q_{min} + \rho(q_{max} - q_{min}) \quad (2)$$

Where:

q_{min}, q_{max} : Minimum and maximum range of motion;

ρ : pseudo-random number in the interval $[0, 1]$ which respects a uniform distribution;

q : the generalized coordinate random value obtained by Monte Carlo method;

This method enables us to obtain a graphical representation of the workspace of the lower limb in the sagittal plane while respecting the joints constraints given in Table 2 as shown in Figure 4. Moreover, the comfort zone is a subset of

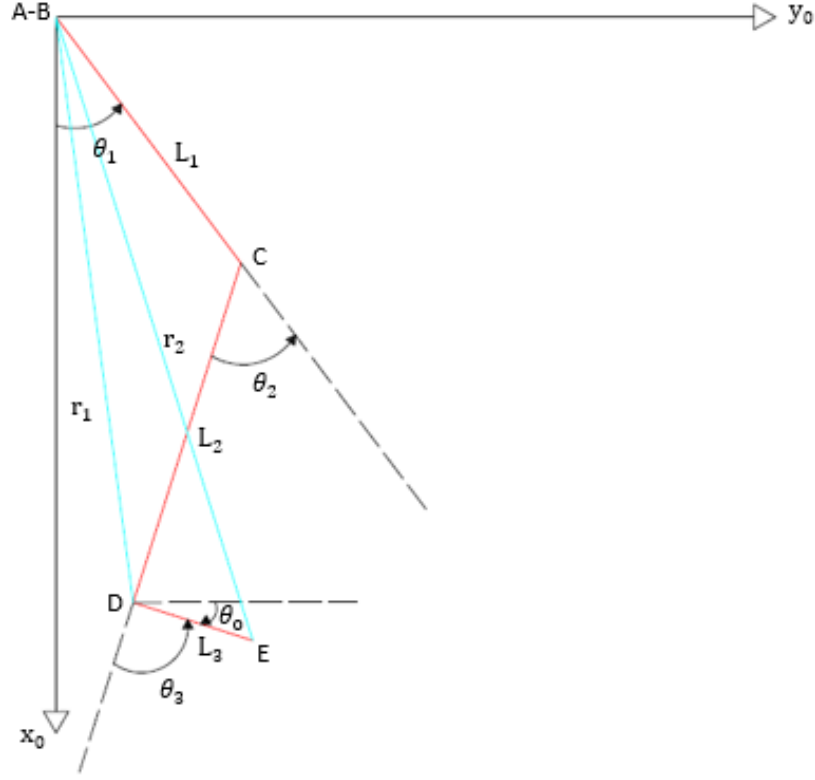


Figure 1: Model of the right lower limb in a sagittal plane

Table 2: Range of motion of the lower limb joints [9]

Joint	θ_i^{min}	θ_i^{max}	Comfort zone	Conditions
i=1	-20°	120°	from 15.75° to 39.55°	knee neutral 0°
i=2	0°	118°	from 0° to 39.55°	hip neutral 0°
i=3	50°	126°	from 77.75° to 103.3°	knee neutral 0°

the corresponding joint range of motion. It is calculated by 35% of the range of motion. While its center, q_c^{comf} , is calculated as follows [9]:

$$q_c^{comf} = \frac{q_{max}^{comf} - q_{min}^{comf}}{2} + q_h^{comf} \quad (3)$$

where q_{max}^{comf} and q_{min}^{comf} are the maximum and the minimum values of the comfort zone, and q_h^{comf} is the home position of for the generalised coordinate q .

Moreover, a trajectory planning is proposed for which the minimum jerk criterion is applied. The jerk approach is considered as the third time derivative of the position. Limiting jerk criterion enables us to ensure the continuity of the acceleration of the joints, which leads to a reduction in the vibrations and to the avoidance of the resonance frequencies [10]. The minimum jerk criteria is obtained by minimizing the function (4).

$$J = \frac{1}{2} \int_0^T \left(\frac{d^3x(t)}{dt^3} \right)^2 dt \quad (4)$$

To satisfy the minimum jerk criteria, the position x is given by a fifth-order polynomial which is interpreted as follows:

$$x(t) = s_0 + s_1t + s_2t^2 + s_3t^3 + s_4t^4 + s_5t^5 \quad (5)$$

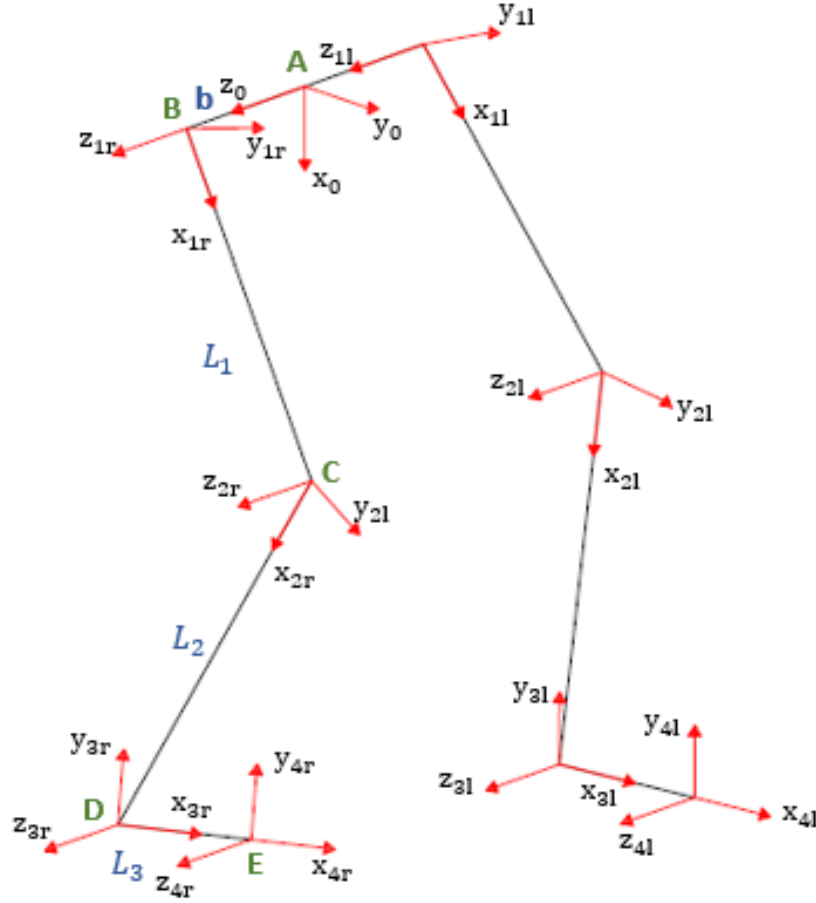


Figure 2: Physiological lower limbs diagram

Using this polynomial, it is possible to specify the position, velocity and acceleration at the beginning and the end of motion. Thus, the final formula is given in Equation (6) [11].

$$\begin{bmatrix} s_0 \\ s_1 \\ s_2 \\ s_3 \\ s_4 \\ s_5 \end{bmatrix} = \begin{bmatrix} 1 & t_0 & t_0^2 & t_0^3 & t_0^4 & t_0^5 \\ 0 & 1 & 2.t_0 & 3.t_0^2 & 4.t_0^3 & 5.t_0^4 \\ 0 & 0 & 2 & 6.t_0 & 12.t_0^2 & 20.t_0^3 \\ 1 & t_f & t_f^2 & t_f^3 & t_f^4 & t_f^5 \\ 0 & 1 & 2.t_f & 3.t_f^2 & 4.t_f^3 & 5.t_f^4 \\ 0 & 0 & 2 & 6.t_f & 12.t_f^2 & 20.t_f^3 \end{bmatrix}^{-1} \begin{bmatrix} x_0 \\ \dot{x}_0 \\ \ddot{x}_0 \\ x_f \\ \dot{x}_f \\ \ddot{x}_f \end{bmatrix} \quad (6)$$

3 Inverse kinematics of the human leg

In [12], generating a trajectory in the joint space allows not only to achieve an effective control of the lower limbs but also to avoid the problems occurring with kinematics singularities. Furthermore, it enables to deal with the problems related to the manipulator redundancy like the proposed human leg model. However, the redundancy allows the lower limbs to avoid kinematics limitations and to minimize energy consumption. Therefore, the inverse kinematics yields the corresponding trajectory in the joint space after generating it in the task space. In our case, the reference system R_0 is considered stationary with respect to an inertial reference frame R_U , in order to avoid an infinite number of solutions. Thus, this section provides different methods for solving the IK of the human leg.

3.1 Analytical method

After having defined the forward kinematics, it is essential to determine the IK. In other words, find the joint angles θ_1 , θ_2 and θ_3 from the predefined coordinate of the end effector $E(E_x, E_y)$ and its orientation relative to the transverse plane θ_0 . Thus, according to Figure 2, the coordinate space of ankle joint D is given as follows:

$$\begin{cases} D_x = E_x - L_3 \cdot S_0 \\ D_y = E_y - L_3 \cdot C_0 \end{cases} \quad (7)$$

Using D-H modified method, the coordinate space of ankle joint is given by:

$$\begin{cases} D_x = L_2 \cdot C_{1-2} + L_1 \cdot C_1 \\ D_y = L_2 \cdot S_{1-2} + L_1 \cdot S_1 \end{cases} \quad (8)$$

Equations (7) and (8), yields to:

$$C_2 = \frac{(E_x - L_3 \cdot S_0)^2 + (E_y - L_3 \cdot C_0)^2 - L_1^2 - L_2^2}{2 \cdot L_1 \cdot L_2} \quad (9)$$

$$S_2 = \pm \sqrt{1 - C_2^2} \quad (10)$$

Then,

$$\theta_2 = \text{atan2}(S_2, C_2) \quad (11)$$

By using this trigonometric equation, we find:

$$\theta_1 = \text{atan2}(E_x - L_3 \cdot S_0, E_y - L_3 \cdot C_0) - \text{atan2}(L_2 \cdot S_2, L_1 + L_2 \cdot C_2) \quad (12)$$

and

$$\theta_3 = \frac{\pi}{2} - \theta_1 + \theta_2 - \theta_0 \quad (13)$$

However, if the orientation angle of the foot is not known, there are multiple possible solutions.

3.2 Numerical methods

3.2.1 Cyclic coordinate descent method

Cyclic Coordinate Descent (CCD) is an algorithm for the iterative solution used to solve inverse kinematics problem. Yotchon et al. [13] presented a combination of the differential evolution algorithm which is a meta heuristic optimization with CCD method to solve the inverse kinematics problem. This method converges to the target whatever the initial condition. CCD consists of minimizing the joint errors by varying one component of the angular vector at a time. This method can be used in real time although it takes several iterations to reach the objective point [14]. One of the main advantages of cyclic coordinate descent is that it is easy to implement. The CCD algorithm consists of measuring the difference between the target and the end-effector vectors. Thereafter, it deduces a rotation matrix to make this difference equal to zero taking into account the joints limitation. This process is repeated for each joint, iterating from the end effector to the root joint of kinematic chains.

3.2.2 Moore-Penrose pseudo-inverse method

Moore-Penrose Pseudo-Inverse method (MPPI) is based on Newton Raphson method which consists on solving the following nonlinear equation:

$$N(q_d) \equiv f(q_d) - p_d = 0 \quad (14)$$

with f is the forward kinematics equation, p_d is the target position and orientation and q is the generalised coordinates. Klein et al. [15], proved that the pseudo inverse IK method is not repeatable. That means the algorithm is not fast computationally and does not yield a minimum norm of angular joint velocities.

To generalize Newton Raphson's procedure, the Taylor expansion of then forward kinematics function is used around q_d as follows :

$$p_d = f(q_d) = f(q_k) + \left. \frac{\partial f}{\partial q} \right|_{q_k} (q_d - q_k) \quad (15)$$

Thus

$$\Delta q = J^+(q_k)(p_d - f(q_k)) \quad (16)$$

Where,

$$J = \frac{\partial f}{\partial q} \quad (17)$$

And J^+ is called the pseudo-inverse of the lower limb's jacobian matrix $J \in \mathbb{R}^{2 \times 3}$ giving by the following expression:

$$J^+ = J^T (J J^T)^{-1} \quad (18)$$

based on (16), an iterative method can be used to calculate the joints update :

$$q_{k+1} = q_k + J^+(q_k)(p_d - f(q_k)) \quad (19)$$

Where q_k and $f(q_k)$ are the generalized coordinates and the end effector position at iteration k, respectively.

3.2.3 Levenberg Marquardt damped least squares method

A method to handle the pseudo-inverse problem uses the Levenberg Marquardt Damped Least Squares method (LMDLS). Wampler et al. [16] proposed a method to choose the optimal damping factor in order to establish a balance between the angular joint velocity and the error. This approach is based on finding the joints angular error vector Δq which minimizes the tracking error and the joint velocities. This corresponds to the minimization of:

$$\|\Delta x - J\Delta q\|^2 - \lambda^2 \|\Delta q\|^2 \quad (20)$$

Where $\lambda > 0$ is the damping factor.

Solving (20), the damped pseudo-inverse $J^{+\lambda}$ is as follows:

$$J^{+\lambda} = J^T (J^T J + \lambda I_{(3 \times 3)})^{-1} \quad (21)$$

Thus the joints' updates are giving by the following equation:

$$q_{i+1} = q_i + J^{+\lambda}(q_i)(p_d - f(q_i)) \quad (22)$$

There are several methods that have been proposed in the literature to select the appropriate and optimum damping factor λ [17], so that the LMDLS method becomes robust against singularity and solvability problems. Among these methods, choose λ as a constant value [18]. To take into consideration the posture of a human, ensuring the natural limits are not exceeded, $q_{min} < q < q_{max}$, the diagonal matrix $\lambda I_{(3 \times 3)}$ will be replaced by $D(\lambda)$, [19].

$$D(\lambda) = \begin{bmatrix} \lambda_1 & 0 & 0 \\ 0 & \lambda_2 & 0 \\ 0 & 0 & \lambda_3 \end{bmatrix} \quad (23)$$

Where $\lambda = [\lambda_1 \quad \lambda_2 \quad \lambda_3]^T$, is defined as follows:

$$\lambda = a \left(\frac{2(q - q_c^{comf})}{q_{max} - q_{min}} \right)^b \quad (24)$$

Where a and b are positive numbers, and q_c^{comf} is the center of the comfort zone for joint configurations q . The limits of the comfort zone are calculated by $0.35 \times$ the limits of the joint range of motion.

Thus, λ imposes a restriction to each joint angular value θ_i , $i \in \{1, 2, 3\}$. If θ_i is within its range of motion mentioned in Table 2, a small value of λ_i yields accurate outcomes; and if the joint value θ_i is close to its limits, a large value of λ_i results in a feasible solution.

3.2.4 Optimization method

Tringali et al. [20] proposed optimal inverse kinematics based on optimization method for a redundant robot manipulator with linear and nonlinear constraints by choosing the appropriate initial conditions. Lu [21] used optimization method to generate feasible and smooth joint motion while detecting collision in space.

Constrained optimization is based on finding an angular vector $q = [\theta_1 \quad \theta_2 \quad \theta_3]^T$, that is a local minimum to the objective function $f(q)$ given as follows:

$$\begin{aligned} f(q) &= |\sqrt{x_d^2 + y_d^2} - r_2| \\ r_2 &= \sqrt{x^2 + y^2} \\ x &= L_3 C_{1-2+3} + L_2 C_{1-2} + L_1 C_1 \\ y &= L_3 S_{1-2+3} + L_2 S_{1-2} + L_1 S_1 \end{aligned} \quad (25)$$

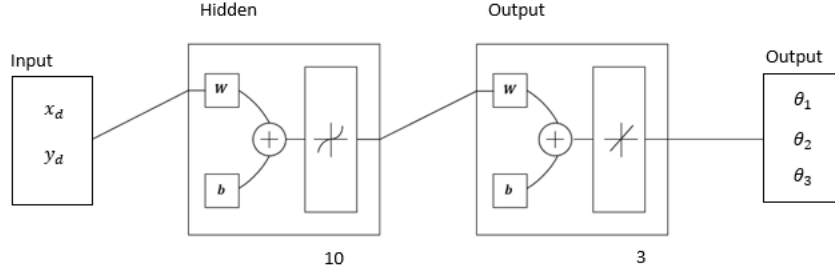


Figure 3: Neural network structure

Where x_d and y_d represent the target position coordinates. The main goal is to identify the realistic configuration by respecting several constraints. One of them is to restrict the angular joint limits. This can be done by using the following barrier function.

$$B_k(q) = f(q) + \frac{1}{k}b(q) \quad (26)$$

This method is called interior point algorithm. When q approaches the boundary, $b(q) \rightarrow +\infty$. Where $b(q)$ is the logarithmic barrier function given by the following expression:

$$b(q) = -(\log(-(q - q_{max})) + \log(-(q_{min} - q))) \quad (27)$$

The other constraints can be expressed as a distance as follows:

$$\begin{cases} x_d = x \\ y_d = y \end{cases} \quad (28)$$

3.2.5 Multi-objective optimization genetic algorithm method

A multi-objective optimization genetic algorithm (MOOGA) is a meta-heuristic algorithm used to solve optimization problems. It is inspired by the evolutionary biology process. Bjoerlykhaug [20] solved IK using optimization with genetic algorithm in real-time as the robot moves, which leads to decrease the computational time to 50%. Solving any optimisation problem using genetic algorithm depends on three main different tasks, namely, initial random population, genetic operators and objective evaluation function.

3.3 Neural networks method

This subsection investigates the neural networks method to find the IK solution for the human leg. Shah et al. [22] adopted deep artificial neural networks to solve the inverse kinematics of a 5-axis serial link robotic manipulator. However, the deviation between the end effector and the target resulting from actuator limitations is around 0.2 mm, which can be reduced by extra training. Demby's et al. [23] evaluated the artificial neural networks performance for solving the IK problem of 4, 5, 6 and 7 DOF robots by using mean square error for the same desired outputs. The authors deduced that the error decreased as the training set increased, which took a long of time to create an effective training.

The neural networks is trained by exploiting the data delivered by the forward kinematics to learn the angular joint values of the configuration space. In other words, the neural networks enables us to identify which joint configuration $q = [\theta_1, \theta_2, \theta_3]^T$ corresponds to the specified end effector position $(x_d, y_d)^T$. Multilayer perceptron is used for solving the inverse kinematics of the lower limb. Its structure is given in Figure 3. It has a two-layer feed-forward network, namely, a hidden layer with 10 interconnected sigmoid normal neurons and an output layer with 3 linear output neurons.

4 Simulation results

This section provides a simulation study of human IK using the methods described above. In order to generate a trajectory as an example, it is necessary to ensure that the starting and final points are in the workspace of the lower

Table 3: Initial and final values for: position, velocity and acceleration of a motion

		x	y
Position (m)	Initial	0.824628	-0.0668736
	Final	0.772227	0.481004
Speed (m/s)	Initial	1.33	1.33
	Final	1.33	1.33
Acceleration (m/s ²)	Initial	0	0
	Final	0	0

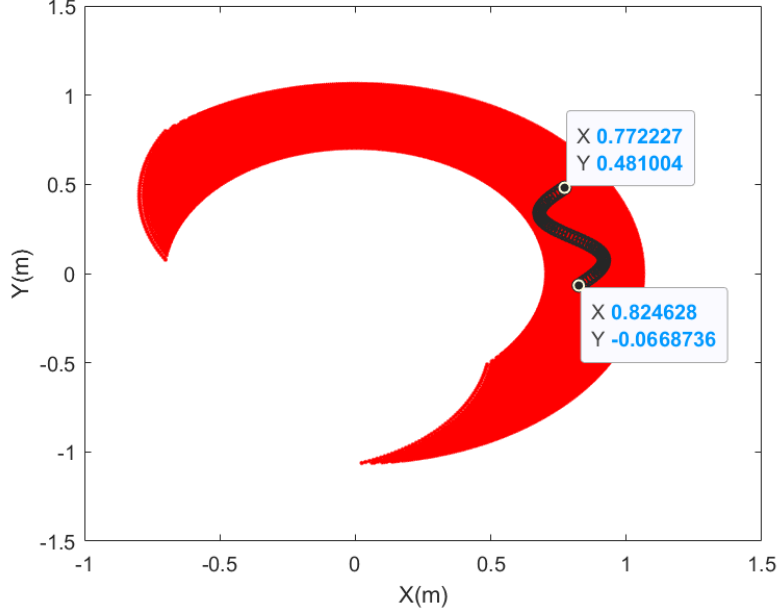


Figure 4: Generated trajectory of the lower limb

limb as described in Figure 4. Based on [24], the average walking speed is between 1 – 1.5 m/s for adults without mobility issues. Then, the velocity and acceleration at the beginning and at the end of motion are 1.33 m/s and 0 m/s^2 respectively in this application example, as shown in Table 3.

Thus, assuming that the movement lasts 0.5 sec . The results of this simulation are illustrated in Figure 4. Using the CCD method, the simulation results of the IK of lower limbs are illustrated in Figure 5. In order to compute the position error shown in Figure 6, these resulting values and the forward kinematics specified in Equation (5) are used to generate the corresponding end effector trajectory. However, according to the simulation realized in Matlab, this method makes links turn in a specific order opposite to reality which makes the movement of the lower limb appears unnatural, hence this method does not take into consideration the physiological potentiality.

While, Figure 7 shows the simulation results of IK of lower limb using MPPI algorithm. As shown in Figure 8, the position error is of the order of 0.04 mm . However, this algorithm does not take into consideration angular constraints. Concerning LMDLS technique, the simulation results are illustrated in Figures 9 and 10. This method shows a high computational cost, which is due to the high complexity of the human leg structure.

Figure 11 shows the resulting angular joint values obtained by applying the optimization algorithm. As shown in Figure 12, the position error is almost zero. This confirms that the optimization technique performs well from the point of view of accuracy.

Using the same objective function and constraints presented in subsection 3.2.4, the joints trajectory and the position error obtained by using the MOOGA technique are depicted in Figures 13 and 14. As can be seen from Figures 13 and 14, the MOOGA technique is an accurate method, but the variation of the angular configurations are abrupt and significant.

Moreover, for using neural network method, out of the 127 282 samples collected, 15% are used for validation, 15% to

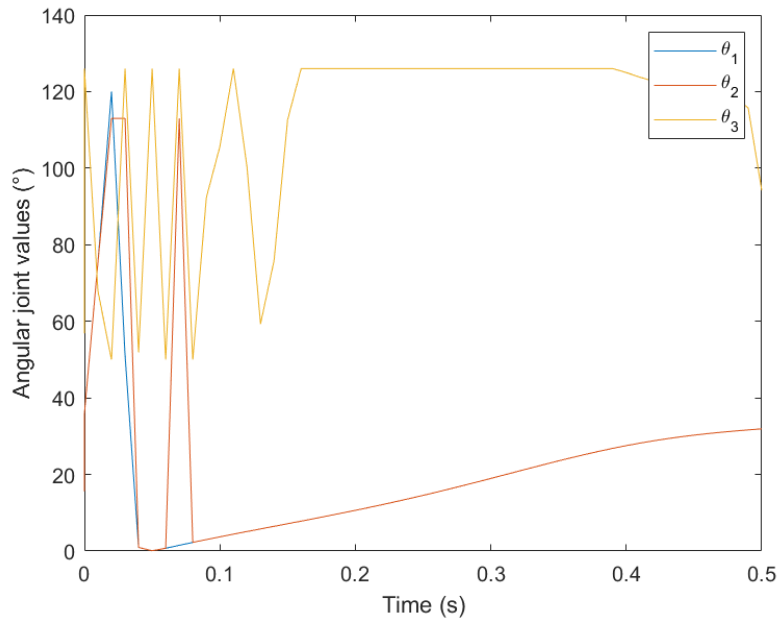


Figure 5: Joints angular tracking using CCD method. For this simulation, $\theta_1^{min} = 0^\circ$, $\theta_1^{max} = 120^\circ$, $\theta_2^{min} = 0^\circ$, $\theta_2^{max} = 117^\circ$, $\theta_3^{min} = 51^\circ$ and $\theta_3^{max} = 126^\circ$.

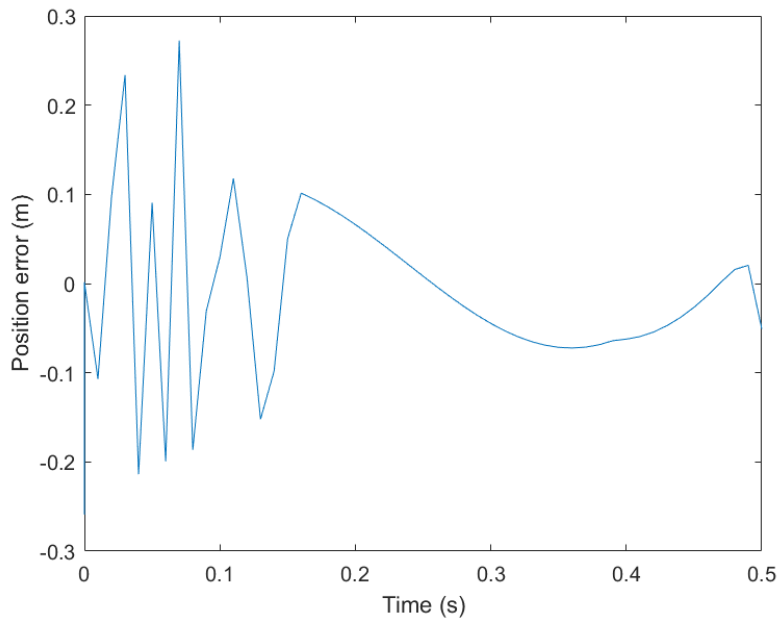


Figure 6: Position error using CCD method

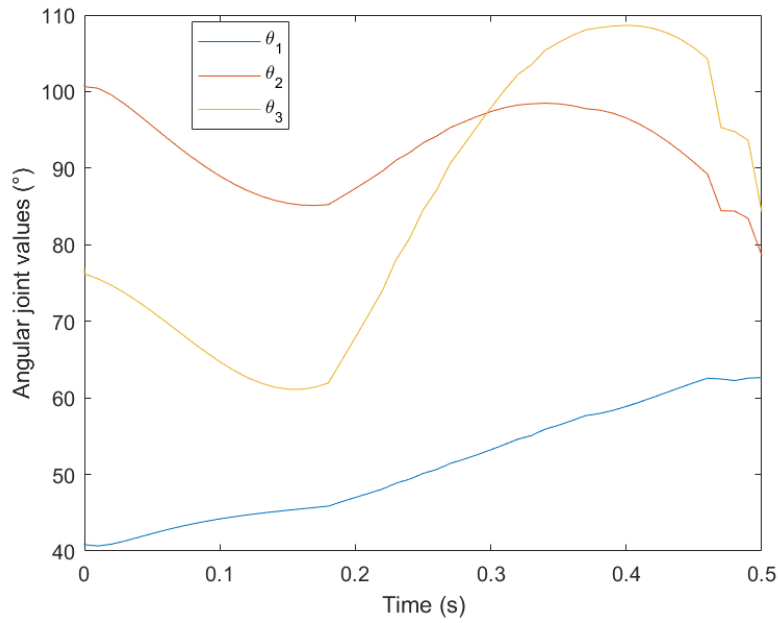


Figure 7: Joints angular tracking using MPPI method. For this simulation, $\theta_1^{min} = 42^\circ$, $\theta_1^{max} = 63^\circ$, $\theta_2^{min} = 79^\circ$, $\theta_2^{max} = 102^\circ$, $\theta_3^{min} = 61^\circ$ and $\theta_3^{max} = 109^\circ$.

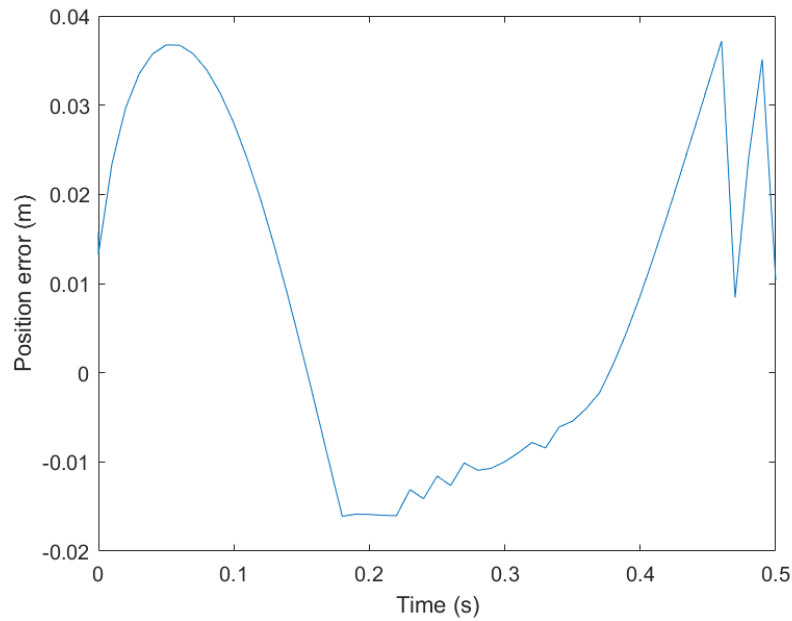


Figure 8: Position error using MPPI method

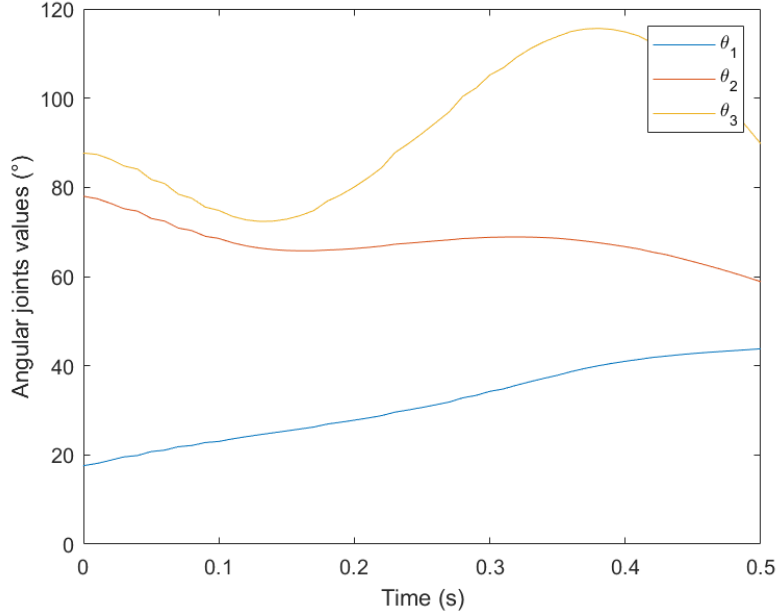


Figure 9: Joints angular tracking using LMDLS method. For this simulation, $\theta_1^{min} = 18^\circ$, $\theta_1^{max} = 43^\circ$, $\theta_2^{min} = 61^\circ$, $\theta_2^{max} = 79^\circ$, $\theta_3^{min} = 87^\circ$ and $\theta_3^{max} = 118^\circ$.

test the neural networks, and 70% of the samples are used for the training of the neural networks. The joint angular values results and the position error are depicted in Figures 15 and 16 respectively. As illustrated in Figure 16, the neural networks technique is an accurate method where the error is less than $1.6 \cdot 10^{-6}$.

5 Discussion

It is inferred from TABLE 4, that neural networks method root mean square position error is less compared to other methods, but optimization and MOOGA methods also show accurate results where root mean square position error is less than 2.10^{-4} . Moreover, CCD and neural networks methods are fast computationally compared to other methods.

$$I_c = mean \left(\underbrace{\xi \sum_{i=1}^3 \left| \frac{d^3 \theta_i(t)}{dt^3} \right|}_{Energy} + \underbrace{\mu D_{CoM} + \beta \sum_{i=1}^3 - (\log(-(\theta_i(t) - \theta_i^{max})) + \log(-(\theta_i^{min} - \theta_i(t))))}_{Robustness} \right) \quad (29)$$

Thereafter, the comfort index I_c shown in Equation (29) is used to evaluate the body posture, and it consists of two components:

- **Energy** : lower limb must satisfy during walking the minimum energy constraint which is related to the minimum jerk approach.
- **Robustness** : the lower limb posture is represented by the generalized coordinates $q = [\theta_1 \ \theta_2 \ \theta_3]^T$, which is constrained by upper and lower limits. Hence, the logarithmic function which is given by Equation (27), increases remarkably when joint angles approach their respective barriers. Besides, the distance between the center of mass of the lower limb and that of whole body given by Equation (30), must be minimal in order to overcome the fatigue and the musculoskeletal discomfort. Let M_i^{seg} and CoM_i represent the mass and the coordinate of the center of mass of segment i , respectively, with $i \in [1, 2, 3]$, then:

$$D_{CoM} = \left| \frac{\sum_{i=1}^3 M_i^{seg} CoM_i}{\sum_{i=1}^3 M_i^{seg}} \right| \quad (30)$$

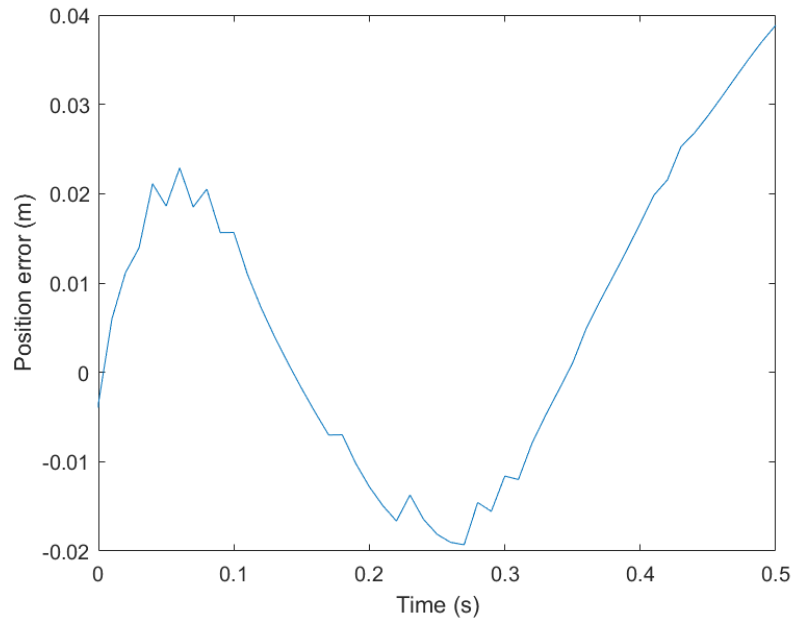


Figure 10: Position error using LMDLS method

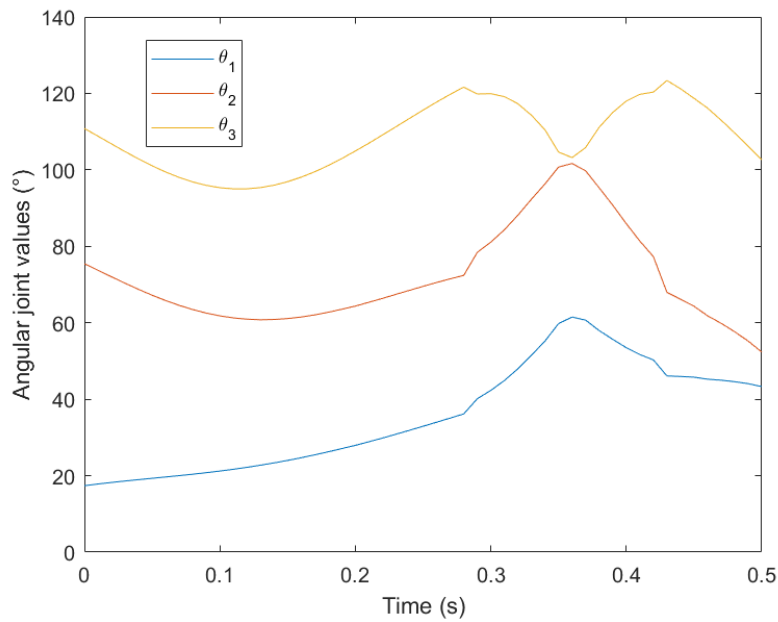


Figure 11: Joints angular tracking using optimisation method. For this simulation, $\theta_1^{min} = 18^\circ$, $\theta_1^{max} = 61^\circ$, $\theta_2^{min} = 52^\circ$, $\theta_2^{max} = 101^\circ$, $\theta_3^{min} = 103^\circ$ and $\theta_3^{max} = 120^\circ$.

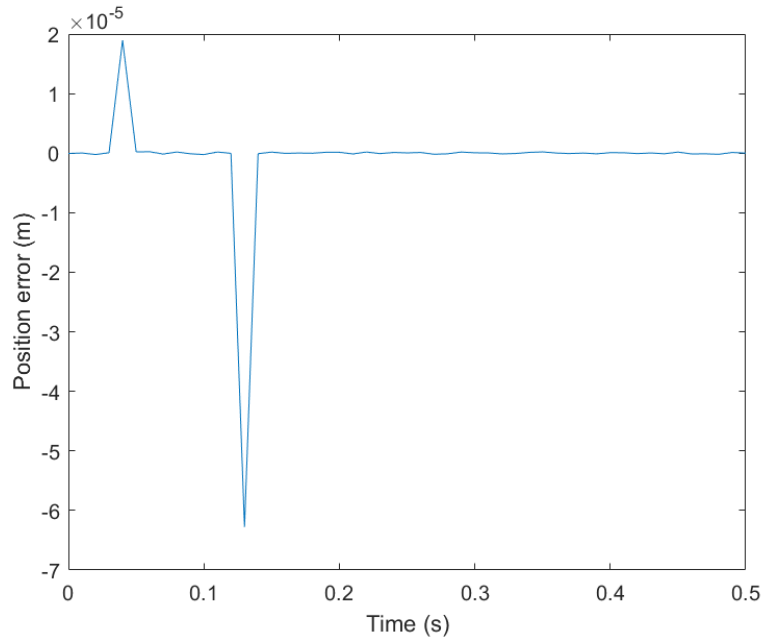


Figure 12: Position error using optimization method

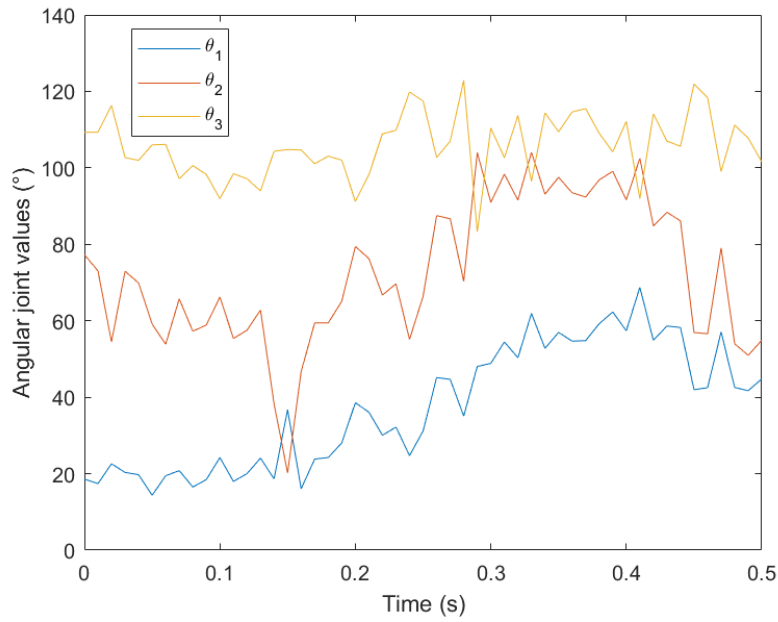


Figure 13: Joints angular tracking using MOOGA method. For this simulation, $\theta_1^{min} = 16^\circ$, $\theta_1^{max} = 68^\circ$, $\theta_2^{min} = 20^\circ$, $\theta_2^{max} = 105^\circ$, $\theta_3^{min} = 84^\circ$ and $\theta_3^{max} = 120^\circ$.

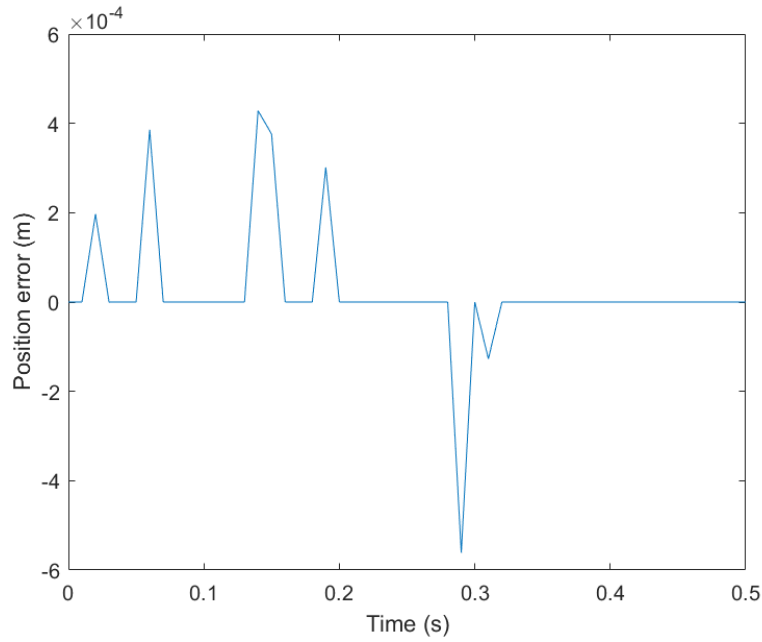


Figure 14: Position error using MOOGA method

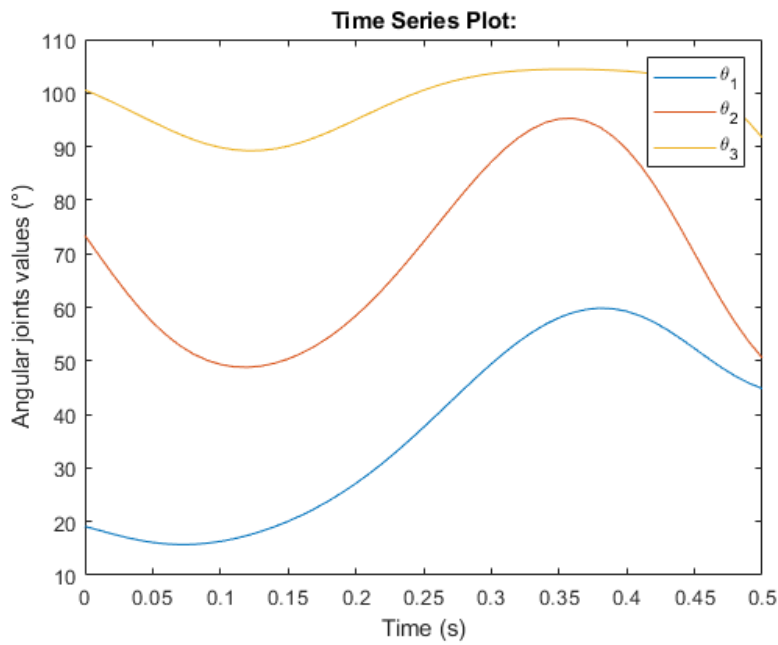


Figure 15: Joints angular tracking using neural network method. For this simulation, $\theta_1^{min} = 15^\circ$, $\theta_1^{max} = 59^\circ$, $\theta_2^{min} = 48^\circ$, $\theta_2^{max} = 95^\circ$, $\theta_3^{min} = 89^\circ$ and $\theta_3^{max} = 104^\circ$.

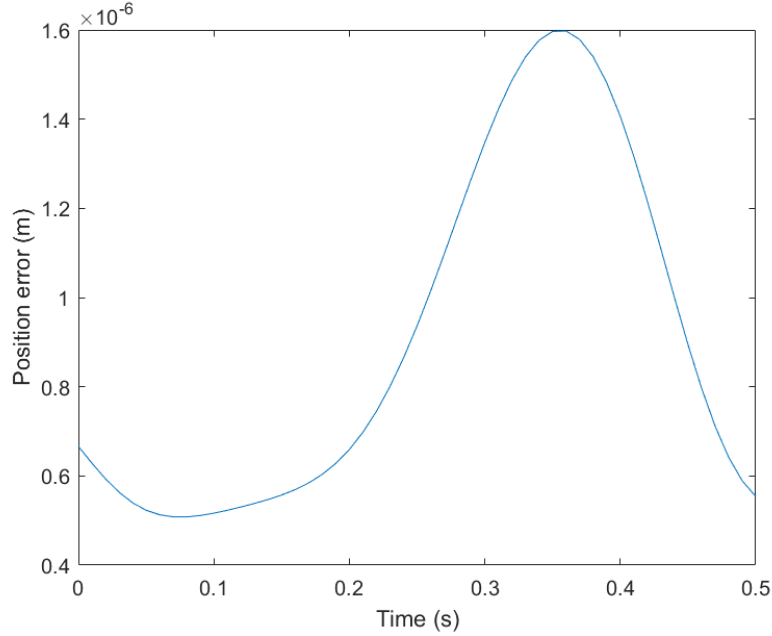


Figure 16: Position error using neural network method

With ξ , μ and β are homogenization of the comfort index coefficients. The results in Tab. 4 show a significantly lower comfort index for neural networks method. For cyclic coordinate descent method, the comfort index goes to infinity because the joint angles are near their limits during the motion as depicted in Figure 5.

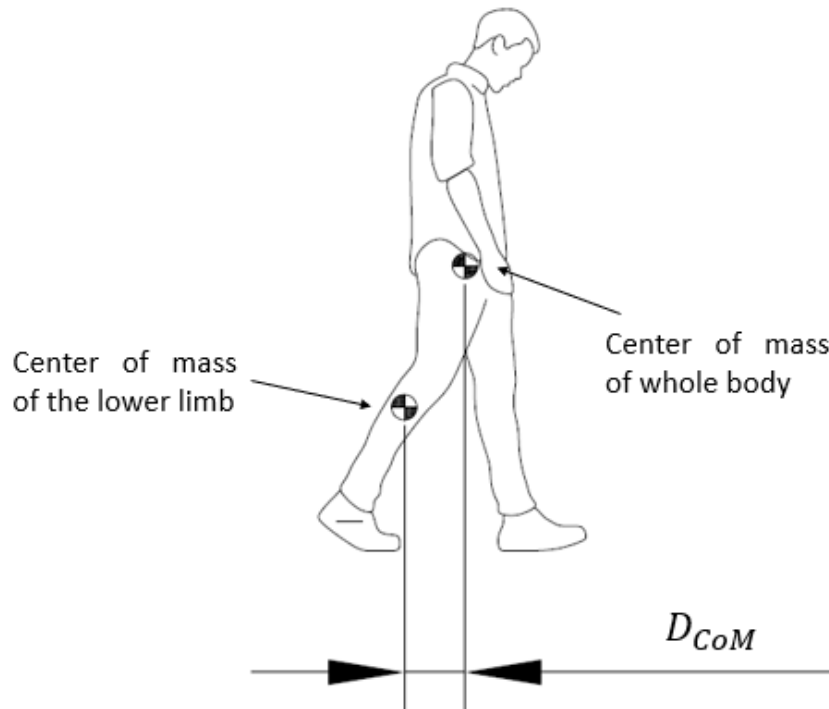


Figure 17: Positions of the centers of mass in human body

Table 4: Comparative table of IK methods

IK method	Computational time (s)	RMSE	I_c
CCD method	0.006101	0.0982	-
MPPI method	2.777852	0.0603	1.1530
LMDLS method	2.051712	0.0299	1.1551
Optimization method	0.0363921	$9.0951 \cdot 10^{-6}$	1.1514
MOOGA method	0.5939144	$1.3407 \cdot 10^{-4}$	1.1577
NN method	0.0082538	$9.7244 \cdot 10^{-7}$	1.0256

6 Conclusion

Throughout this paper, a comparative study of human inverse kinematics techniques for lower limbs was presented. Theoretical results showed that the neural networks method is the most efficient compared to all the other methods considered in terms of root mean square position error, computational time and production of realistic posture. Indeed, human comfort during motion is affected by physiological factors including energy consumption, joint angles limits and the distance between center of mass of the lower limb and that of whole body. Also, comfort posture is impacted by environment and psychological factors that are not taken into consideration in this paper.

References

- [1] Dongsheng Zhou, Lu Ji, Qiang Zhang, and Xiaopeng Wei. Practical analytical inverse kinematic approach for 7-dof space manipulators with joint and attitude limits. *Intelligent Service Robotics*, 8(4):215–224, 2015.
- [2] João Carlos Alves Barata and Mahir Saleh Hussein. The moore–penrose pseudoinverse: A tutorial review of the theory. *Brazilian Journal of Physics*, 42(1-2):146–165, 2012.
- [3] Ben Kenwright. Inverse kinematics–cyclic coordinate descent (ccd). *Journal of Graphics Tools*, 16(4):177–217, 2012.
- [4] Samuel R Buss. Introduction to inverse kinematics with jacobian transpose, pseudoinverse and damped least squares methods. *IEEE Journal of Robotics and Automation*, 17(1-19):16, 2004.
- [5] Sergiu-Dan Stan, Vistrian Maties, and Radu Balan. Genetic algorithms multiobjective optimization of a 2 dof micro parallel robot. In *2007 International Symposium on Computational Intelligence in Robotics and Automation*, pages 522–527. IEEE, 2007.
- [6] Raşit Köker, Cemil Öz, Tarık Çakar, and Hüseyin Ekiz. A study of neural network based inverse kinematics solution for a three-joint robot. *Robotics and autonomous systems*, 49(3-4):227–234, 2004.
- [7] Blandine Calais-Germain. *Anatomy of movement*. Eastland Press, 1993.
- [8] Ilya M Sobol. *A primer for the Monte Carlo method*. CRC press, 2018.
- [9] Sebastian Głowiński and Tomasz Krzyżyński. An inverse kinematic algorithm for the human leg. *Journal of theoretical and Applied Mechanics*, 54(1):53–61, 2016.
- [10] Alessandro Gasparetto, Paolo Boscariol, Albano Lanzutti, and Renato Vidoni. Path planning and trajectory planning algorithms: A general overview. *Motion and operation planning of robotic systems*, pages 3–27, 2015.
- [11] John J Craig. *Introduction to robotics: mechanics and control*. Pearson Educacion, 2005.
- [12] Alessandro Gasparetto, Paolo Boscariol, Albano Lanzutti, and Renato Vidoni. Path planning and trajectory planning algorithms: A general overview. *Motion and operation planning of robotic systems*, pages 3–27, 2015.
- [13] Phanomphon Yotchon and Yutana Jewajinda. Combining a differential evolution algorithm with cyclic coordinate descent for inverse kinematics of manipulator robot. In *2021 3rd International Conference on Electronics Representation and Algorithm (ICERA)*, pages 35–40. IEEE, 2021.
- [14] Ben Kenwright. Inverse kinematics–cyclic coordinate descent (ccd). *Journal of Graphics Tools*, 16(4):177–217, 2012.
- [15] Charles A Klein and Ching-Hsiang Huang. Review of pseudoinverse control for use with kinematically redundant manipulators. *IEEE Transactions on Systems, Man, and Cybernetics*, pages 245–250, 1983.
- [16] Charles W Wampler. Manipulator inverse kinematic solutions based on vector formulations and damped least-squares methods. *IEEE Transactions on Systems, Man, and Cybernetics*, 16(1):93–101, 1986.

- [17] Arati S Deo and Ian D Walker. Overview of damped least-squares methods for inverse kinematics of robot manipulators. *Journal of Intelligent and Robotic Systems*, 14(1):43–68, 1995.
- [18] Charles W Wampler. Manipulator inverse kinematic solutions based on vector formulations and damped least-squares methods. *IEEE Transactions on Systems, Man, and Cybernetics*, 16(1):93–101, 1986.
- [19] Marian G Alvarez-Perez, Mario A Garcia-Murillo, and J Jesús Cervantes-Sánchez. Robot-assisted ankle rehabilitation: a review. *Disability and Rehabilitation: Assistive Technology*, 15(4):394–408, 2020.
- [20] Emil Dale Bjoerlykhaug. A closed loop inverse kinematics solver intended for offline calculation optimized with ga. *Robotics*, 7(1):7, 2018.
- [21] Yao-An Lu, Kai Tang, and Cheng-Yong Wang. Collision-free and smooth joint motion planning for six-axis industrial robots by redundancy optimization. *Robotics and Computer-Integrated Manufacturing*, 68:102091, 2021.
- [22] Shubham Kamlesh Shah, Ruby Mishra, and Lala Samprit Ray. Solution and validation of inverse kinematics using deep artificial neural network. *Materials Today: Proceedings*, 26:1250–1254, 2020.
- [23] Shubham Kamlesh Shah, Ruby Mishra, and Lala Samprit Ray. Solution and validation of inverse kinematics using deep artificial neural network. *Materials Today: Proceedings*, 26:1250–1254, 2020.
- [24] Marc Fisher. *Handbook of Clinical Neurology Volume 92, Stroke Part I: Basic and Epidemiological Aspects*. Elsevier, 2009.